Inorg. Chem. **2006**, *45*, 1508–1516

Two Three-Dimensional Metal–Organic Frameworks Containing One-Dimensional Hydroxyl/Carboxylate Mixed Bridged Metal Chains: Syntheses, Crystal Structures, and Magnetic Properties

Xiao-Ju Li,[†] Xin-Yi Wang,[‡] Song Gao,*[,‡] and Rong Cao*[,†]

State Key Laboratory of Structural Chemistry, Fujian Institute of Research on the Structure of Matter, The Chinese Academy of Sciences, Fuzhou, Fujian 350002, P. R. China, State Key Laboratory of Rare Earth Materials Chemistry and Applications, College of Chemistry and Molecular Engineering, Peking University, Beijing 100871, P. R. China

Received June 19, 2005

Two novel three-dimensional complexes formulated as $[M_3(bime)_2(\mu_3\text{-}OH)_2(HO\text{–}BDC)_2]_n$ (M = Co, **1**; Cu, **2**) [bime = 1,2-bis(imidazol-1′-yl)ethane, HO–H_2BDC = 5-hydroxyisophthalic acid] have been hydrothermally synthesized and characterized. Both **1** and **2** exhibit similar structural frameworks resulting from one-dimensional metal/oxygen chains extended by HO–BDC, but the bridging modes of HO–BDC and coordination environments of metal centers are different. Complexes **1** and **2** crystallize in the orthorhombic system, space group *Pbcn*, a = 18.458(2) [18.2119(12) for **2**] Å, b = 12.0616(14) [11.6847(7)] Å, c = 11.4859(14) [12.0688(6)] Å, and Z = 4 (4). Magnetic studies show that **1** displays a slow magnetic relaxation, a large hysteresis, and distinct finite-size effects and **2** contains an antiferromagnetic chain.

Introduction

Considerable efforts have been devoted to the syntheses and investigation of zero- and one-dimensional magnetic materials as so-called single-molecule magnets (SMMs) and single-chain magnets (SCMs),[1,2] as well as high-dimensional metal−organic hybrid materials containing paramagnetic metal ions. The motivation in these fields is justified not only by the intellectual challenge of understanding the fundamental correlation between structures and magnetic properties, but also by the development of new types of functional molecule-based magnetic materials.[3−6] The common synthetic route to build such magnetic architectures is to utilize appropriate bridging ligands with functional groups and specific spacers. The functional groups in the ligands are capable of transmitting magnetic exchanges and of binding to metal centers through specific coordination modes. The spacers between coordination sites not only can separate the metal clusters or chains to reduce the magnetic coupling between them, but also can stretch the metal building units into esthetically pleasing frameworks.[3−6] In this respect, carboxylates as efficient superexchange pathways between metal ions have received extensive attention. First, carboxylates can adopt versatile coordination conformations, from

* To whom correspondence should be addressed. E-mail: gaosong@pku.edu.cn (S.G.), rcao@fjirsm.ac.cn (R.C.). Fax: +86-591-83714946.
† The Chinese Academy of Sciences.
‡ Peking University.

(1) (a) Wernsdorfer, W.; Aliaga-Alcalde, N.; Hendrickson, D. N.; Christou, G. *Nature* **2002**, *416*, 406. (b) Gatteschi, D.; Sessoli, R. *Angew. Chem., Int. Ed.* **2003**, *42*, 268 and references therein.
(2) (a) Caneschi, A.; Gatteschi, D.; Lalioti, N.; Sangregorio, C.; Sessoli, R.; Venturi, G.; Vindigni, A.; Rettori, A.; Pini, M. G.; Novak, M. A. *Angew. Chem., Int. Ed.* **2001**, *40*, 1760. (b) Clérac, R.; Miyasaka, H.; Yamashita, M.; Coulton, C. *J. Am. Soc. Chem.* **2002**, *124*, 12837. (c) Lescouëzec, R.; Vaissermann, J.; Ruiz-Pérez, C.; Lloret, F.; Carrasco, R.; Julve, M.; Verdaguer, M.; Dromzee, Y.; Gatteschi, D.; Wernsdorfer, W. *Angew. Chem., Int. Ed.* **2003**, *42*, 1483. (d) Liu, T. F.; Fu, D.; Gao, S.; Zhang, Y. Z.; Sun, H. L.; Su, G.; Liu, Y. J. *J. Am. Chem. Soc.* **2003**, *125*, 13976. (e) Wang, S.; Zuo, J. L.; Gao, S.; Song, Y.; Zhou, H. C.; Zhang, Y. Z.; You, X. Z. *J. Am. Soc. Chem.* **2004**, *126*, 8900.
(3) Kahn, O. *Molecular Magnetism*; VCH: Weinheim, Germany, 1993.
(4) (a) Humphrey, S. M.; Mole, R. A.; Rawson, J. M.; Wood, P. T. *Dalton Tran.* **2004**, 1670. (b) Hong, C. S.; Son, S. K.; Lee, Y. S.; Jun, M. J.; Do, Y. *Inorg. Chem.* **1999**, *38*, 5602. (c) Hao, X.; Wei, Y.; Zhang, S. *Chem. Commun.* **2000**, 2271.
(5) (a) Gutschke, S. O. H.; Price, D. J.; Powell, A. K.; Wood, P. T. *Angew. Chem., Int. Ed.* **2001**, *40*, 1920. (b) Konar, S.; Mukherjee, P. S.; Zangrando, E.; Lloret, F.; Chaudhuri, N. R. *Angew. Chem., Int. Ed.* **2002**, *41*, 1561. (c) Tynan, E.; Jensen, P.; Kelly, N. R.; Kruger, P. E.; Lees, A. C.; Moubaraki, B.; Murray, K. S. *Dalton Tran.* **2004**, 3440. (d) Wang, S. B.; Yang, G. M.; Li, R. F.; Wang, Y. F.; Liao, D. Z. *Eur. J. Inorg. Chem.* **2004**, 4907.
(6) (a) Gao, E. Q.; Yue, Y. F.; Bai, S. Q.; He, Z.; Yan, C. H. *J. Am. Chem. Soc.* **2004**, *126*, 1419. (b) Jiang, Y. C.; Wang, S. L.; Lee, S. F.; Lii, K. H. *Inorg. Chem.* **2003**, *42*, 6154. (c) Gutschke, S. O. H.; Price, D. J.; Powell, A. K.; Wood, P. T. *Eur. J. Inorg. Chem.* **2001**, 2739.

10.1021/ic050999x CCC: $33.50
Published on Web 01/13/2006

Chart 1. 1,2-Bis(imidazol-1′-yl)ethane (bime)

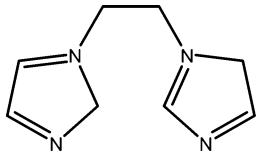

terminal monodentate to various bridging modes (e.g., syn−syn, syn−anti, anti−anti), to which the magnetic exchanges are closely related.[7] Second, carboxylates can generate metal−oxygen chains or polynuclear clusters, which are excellent candidates for magnetic materials, as manifested in some remarkable examples: a 3D homometallic ferrimagnet based on fused Ni(II) octahedral chains and two compounds built on magnetic Δ chains.[5a,5b] Third, the strong coordination ability of carboxylates can result in thermal stability of the compounds. Accordingly, many ferromagnetic, antiferromagnetic, and metamagnetic materials have been prepared using carboxylates as functional groups.[5−8] However, reports on high-dimensional homometallic ferrimagnetic examples are still rare, because the pursuit of appropriate conditions in such systems is difficult. Our group[9] and some other groups[7b,10] have recently attempted to introduce a second type of ligand into the metal carboxylate system to formulate these extended complexes. In comparison to the pyridyl-containing bridging ligands extensively used as secondary ligands in the construction of high-dimensional magnetic complexes,[11] we have selected a flexible imidazolyl-containing ligand, 1,2-bis(imidazol-1′-yl)ethane (bime) (Chart 1) as an assistant ligand. Its flexibility and conformational freedom can result not only in gauche and anti conformations inducing supramolecular isomerism in coordination, but also in free rotation to meet the requirements of the coordination geometry of the metal ions in the assembly process.[12] Thus, bime might favor the further minimization of intercluster or interchain magnetic exchanges joined by carboxylates and the elongation of the metal building units into higher-dimensional frameworks. In this article, we report the syntheses, crystal structures, and magnetic behaviors of two three-dimensional metal−organic complexes, $[M_3(bime)_2(\mu_3\text{-}OH)_2(HO{-}BDC)_2]_n$ (M = Co, **1**; Cu, **2**) (HO−H_2BDC = 5-hydroxyisophthalic acid), in which hydroxyl/carboxylate mixed bridged metal chains are well isolated. Magnetic measurements reveal that **1** shows a superparamagnetic-like behavior with alternating F/AF/AF ferrimagnetic chains, whereas **2** presents an overall antiferromagnetic chain behavior.

Experimental Section

Materials. 1,2-Bis(imidazol-1′-yl)ethane was synthesized according to the literature method.[12] 5-Hydroxyisophthalic acid was purchased from Aldrich and used without further purification; all other reagents were commercially available and were used as purchased.

Physical Measurements. Elemental analyses of C, H, and N were performed using a Perkin-Elmer 240C elemental analyzer. IR spectra as KBr pellets were recorded on a Magna 750 FT-IR spectrophotometer. The measurements of variable-temperature magnetic susceptibility, zero-field ac magnetic susceptibility, and field dependence of magnetization were carried out on an Oxford Maglab2000 System and a Quantum Design MPMS-XL5 SQUID magnetometer. The experimental susceptibilities were corrected for diamagnetism (Pascal's tables).

Preparation of $[Co_3(bime)_2(\mu_3\text{-}OH)_2(HO{-}BDC)_2]_n$ (1). A mixture of 1,2-bis(imidazol-1′-yl)ethane (0.25 mmol, 40.5 mg), 5-hydroxyisophthalic acid (0.25 mmol, 45.5 mg), NaOH (0.50 mmol, 20.0 mg), and $Co(NO_3)_2{\cdot}6H_2O$ (0.25 mmol, 72.8 mg) in distilled water (18 mL) was placed in a Teflon-lined stainless steel vessel, heated to 170 °C for 4 days, and then cooled to room temperature over 24 h. Deep red block crystals of **1** were obtained, washed with methanol and ether, and dried in a vacuum (yield 37.9 mg, 62% based on Co). Elemental analysis (%): calcd for $C_{24}H_{20}Co_3N_4O_{12}$ C 39.31, H 2.75, N 7.64; found C 38.64, H 3.01, N 7.27. IR (KBr, cm^{-1}): 3157 m, 3126 m, 1556 s, 1470 w, 1442 m, 1404 s, 1375 s, 1303 w, 1267 m, 1236 w, 1111 m, 1091 m, 1002 w, 979 w, 856 w, 782 m, 754 w, 720 m, 661 w.

Preparation of $[Cu_3(bime)_2(\mu_3\text{-}OH)_2(HO{-}BDC)_2]_n$ (2). The procedure is similar to the synthesis of **1** except that $Co(NO_3)_2{\cdot}6H_2O$ was replaced by $Cu(NO_3)_2{\cdot}3H_2O$ (0.25 mmol, 60.4 mg). Blue block crystals of **2** were obtained (yield 34.9 mg, 56% based on Cu). Elemental analysis (%): calcd for $C_{24}H_{20}Cu_3N_4O_{12}$ C 38.59, H 2.70, N 7.50; found C 38.50, H 2.86, N 7.33. IR (KBr, cm^{-1}): 3153 m, 3131 m, 1555 s, 1474 w, 1443 m, 1417 s, 1378 s, 1301 w, 1268 m, 1222 w, 1115 m, 1096 m, 1003 w, 976 w, 853 w, 779 m, 754 w, 722 m, 656 w.

Crystal Structure Determinations. Intensity data for **1** and **2** were measured on a Siemens Smart CCD diffractometer with graphite-monochromated Mo Kα radiation (λ = 0.71073 Å) at 293(2) K.[13] The structures were solved by direct methods using the SHELXS-97 programs[14] and refined on F^2 by full-matrix least-squares using the SHELXL-97 program package.[15] The positions of H atoms were generated geometrically (C−H bond fixed at 0.96 Å), assigned isotropic thermal parameters, and allowed to ride on their parent carbon atoms before the final cycle of refinement. Crystal data and structure determination summaries for **1** and **2** are listed in Table 1. Selected bond lengths and angles for the two compounds are listed in Tables 2 and 3. Crystallographic data (excluding structure factors) for the two structures have been

(7) (a) Dey, S. K.; Bag, B.; Abdul Malik, K. M.; Salah El Fallah, M.; Ribas, J.; Mitra, S. *Inorg. Chem.* **2003**, *42*, 4029. (b) Maji, T. K.; Sain, S.; Mostata, G.; Lu, T. H.; Ribas, J.; Montort, M.; Chaudhuri, N. R. *Inorg. Chem.* **2003**, *42*, 709.
(8) (a) Chen, H. J.; Mao, Z. W.; Gao, S.; Chen, X. M. *Chem. Commun.* **2001**, 2320. (b) Wang, R. H.; Gao, E. Q.; Hong, M. C.; Gao, S.; Luo, J. H.; Lin, Z. Z.; Han, L.; Cao, R. *Inorg. Chem.* **2003**, *42*, 5486.
(9) (a) Wang, X. Y.; Wei, H. Y.; Wang, Z. M.; Chen, Z. D.; Gao, S. *Inorg. Chem.* **2005**, *44*, 572. (b) Li, X. J.; Cao, R.; Sun, D. F.; Bi, W. H.; Wang, Y. Q.; Li, X.; Hong, M. C. *Cryst. Growth Des.* **2004**, *4*, 775.
(10) (a) Zheng, Y. Q.; Lin, J. L.; Kong, Z. P. *Inorg. Chem.* **2004**, *43*, 2590. (b) Almeida Paz, F. A.; Klinowski, J. *Inorg. Chem.* **2004**, *43*, 3948. (c) Tao, J.; Tong, M. L.; Chen, X. M. *J. Chem. Soc., Dalton Trans.* **2000**, 3669.
(11) (a) Mukherjee, P. S.; Konar, S.; Zangrando, E.; Mallah, T.; Ribas, J.; Chaudhuri, N. R. *Inorg. Chem.* **2003**, *42*, 2695. (b) Gotzone Barandika, M.; Hernández-Pino, M. L.; Karmele Urtiaga, M.; Cortés, R.; Lezama, L.; Isabel Arriortua, M.; Rojo, T. *J. Chem. Soc., Dalton Trans*. **2000**, 1469.
(12) Wu, L. P.; Yamagiwa, Y.; Kuroda-Sowa, T.; Kamikawa, T.; Munakata, M. *Inorg. Chim. Acta* **1997**, *256*, 155.
(13) Sheldrick, G. M. *SADABS, Program for Empirical Absorption Correction of Area Detector Data*; University of Göttingen: Göttingen, Germany, 1996.
(14) Sheldrick, G. M. *SHELXS 97, Program for Crystal Structure Solution*; University of Göttingen: Göttingen, Germany, 1997.
(15) Sheldrick, G. M. *SHELXL 97, Program for Crystal Structure Refinement*; University of Göttingen: Göttingen, Germany, 1997.

Table 1. Crystal Data and Structure Determination Summaries for **1** and **2**

	1	**2**
formula	$C_{24}H_{20}Co_3N_4O_{12}$	$C_{24}H_{20}Cu_3N_4O_{12}$
fw	733.22	747.06
crystal size (mm)	0.20 × 0.18 × 0.12	0.12 × 0.10 × 0.10
crystal system	orthorhombic	orthorhombic
space group	*Pbcn*	*Pbcn*
A (Å)	18.458(2)	18.2119(12)
b (Å)	12.0616(14)	11.6847(7)
c (Å)	11.4859(14)	12.0688(6)
V (Å^3)	2557.2(5)	2568.2(3)
Z	4	4
D_c (g cm^{-3})	1.905	1.932
μ (mm^{-1})	2.000	2.538
T/K	293(2)	293(2)
λ (Mo Kα) (Å)	0.71073	0.71073
reflections collected	5823	5881
unique reflections	2233	2240
R_{int}	0.0561	0.0719
parameters	235	235
S on F^2	0.947	0.924
R1 [$I > 2\sigma(I)$][a]	0.0447	0.0490
wR2 ($I > 2\sigma(I)$][b]	0.1174	0.1180
R1 (all data)[a]	0.0859	0.0939
wR2 (all data)[b]	0.1485	0.1480
$\Delta\rho_{min}$ and $\Delta\rho_{max}$ (ϵ/Å^3)	0.590 and −0.567	0.493 and −0.635

[a] $R = \sum||F_o| - |F_c||)/\sum|F_o|$. [b] $wR = [\sum w(F_o^2 - F_c^2)^2/\sum w(F_o^2)^2]^{1/2}$.

Table 2. Selected Bond Lengths (Å) and Angles (deg) for Complex **1**[a]

Co(1)−O(1)	2.057(4)	Co(2)−O(3)$^{\#2}$	2.043(4)
Co(1)−O(2)	2.269(4)	Co(2)−N(1)	2.067(5)
Co(1)−O(5)$^{\#3}$	2.035(4)	Co(2)−O(1)	2.095(4)
Co(2)−O(1)$^{\#1}$	1.994(4)	Co(2)−O(2)	2.107(4)
O(5)$^{\#3}$−Co(1)−O(5)$^{\#4}$	97.9(2)	O(1)$^{\#1}$−Co(2)−N(1)	101.18(17)
O(5)$^{\#3}$−Co(1)−O(1)	95.25(16)	O(3)$^{\#2}$−Co(2)−N(1)	90.72(17)
O(5)$^{\#4}$−Co(1)−O(1)	96.08(15)	O(1)$^{\#1}$−Co(2)−O(1)	82.48(16)
O(1)−Co(1)−O(1)$^{\#2}$	162.7(2)	O(3)$^{\#2}$−Co(2)−O(1)	88.19(15)
O(5)$^{\#3}$−Co(1)−O(2)	90.36(14)	N(1)−Co(2)−O(1)	175.38(16)
O(5)$^{\#4}$−Co(1)−O(2)	169.59(14)	O(1)$^{\#1}$−Co(2)−O(2)	102.16(15)
O(1)−Co(1)−O(2)	76.78(14)	O(3)$^{\#2}$−Co(2)−O(2)	114.22(15)
O(1)−Co(1)−O(2)$^{\#2}$	90.12(14)	N(1)−Co(2)−O(2)	96.72(16)
O(2)−Co(1)−O(2)$^{\#2}$	82.18(19)	O(1)−Co(2)−O(2)	79.66(14)
O(1)$^{\#1}$−Co(2)−O(3)$^{\#2}$	140.08(16)		

[a] Symmetry transformations used to generate equivalent atoms: #1 $-x + 1, -y + 1, -z$; #2 $-x + 1, y, -z + {}^1/_2$; #3 $-x + {}^1/_2, y + {}^1/_2, z$; #4 $x + {}^1/_2, y + {}^1/_2, -z + {}^1/_2$.

Table 3. Selected Bond Lengths (Å) and Angles (deg) for Complex **2**[a]

Cu(1)−O(5)$^{\#3}$	1.973(4)	Cu(1)−O(5)$^{\#2}$	1.973(4)
Cu(1)−O(2)	2.024(4)	Cu(2)−O(1)	1.914(5)
Cu(1)−O(2)$^{\#4}$	2.024(4)	Cu(2)−O(1)$^{\#1}$	1.922(5)
Cu(1)−O(1)$^{\#4}$	2.336(5)	Cu(2)−O(3)$^{\#1}$	1.942(4)
Cu(1)−O(1)	2.336(5)	Cu(2)−N(1)	1.974(6)
O(5)$^{\#2}$−Cu(1)−O(5)$^{\#3}$	91.2(3)	O(1)−Cu(2)−O(1)$^{\#1}$	80.6(2)
O(5)$^{\#2}$−Cu(1)−O(2)	175.03(18)	O(1)−Cu(2)−O(3)$^{\#1}$	158.6(2)
O(5)$^{\#3}$−Cu(1)−O(2)	87.93(19)	O(1)$^{\#1}$−Cu(2)−O(3)$^{\#1}$	92.9(2)
O(2)−Cu(1)−O(2)$^{\#4}$	93.4(3)	O(1)−Cu(2)−N(1)	99.1(2)
O(5)$^{\#2}$−Cu(1)−O(1)	93.80(18)	O(1)$^{\#1}$−Cu(2)−N(1)	168.5(2)
O(5)$^{\#3}$−Cu(1)−O(1)	94.84(18)	O(3)$^{\#1}$−Cu(2)−N(1)	91.2(2)
O(2)−Cu(1)−O(1)	91.14(18)		
O(2)$^{\#4}$−Cu(1)−O(1)	80.35(18)		
O(1)$^{\#4}$−Cu(1)−O(1)	167.6(3)		

[a] Symmetry transformations used to generate equivalent atoms: #1 $-x, -y, -z + 1$; #2 $x + {}^1/_2, y + {}^1/_2, -z + {}^1/_2$; #3 $-x - {}^1/_2, y + {}^1/_2, z$; #4 $-x, y, -z + {}^1/_2$.

deposited in the Cambridge Crystallographic Data Center, with accession numbers 251451 for **1** and 251452 for **2**. Copies of the data can be obtained free of charge upon application to the CCDC, 12 Union Road, Cambridge CB2 1EZ, U.K. [fax (international) +44-1223/336-033, e-mail deposit@ccdc.cam.ac.uk].

Results and Discussion

Synthesis. The hydrothermal method has been extensively explored as an effective and powerful tool in the self-assembly of metal−organic coordination polymers, especially for high-dimensional frameworks, even though its reaction mechanism is not clear.[16] As known, many transition metal carboxylate compounds have been successfully prepared under hydrothermal conditions, which might be due to the poor solubility of carboxylate ligands.[17] In this article, compounds **1** and **2** were also isolated under hydrothermal conditions. Deep red block crystals of **1** were obtained from the hydrothermal reaction of $Co(NO_3)_2{\cdot}6H_2O$, bime, HO−H_2BDC, and NaOH (1:1:1:2), and blue block crystals of **2** were generated when $Co(NO_3)_2{\cdot}6H_2O$ was replaced by $Cu(NO_3)_2{\cdot}3H_2O$ under the same conditions.

IR Spectroscopy. The IR spectra of complexes **1** and **2** contain characteristic peaks of hydroxyl group (−OH) of HO−BDC at 3126 and 3131 cm^{-1}, respectively. The characteristic bands of the carboxylate group in **1** appear at 1556 cm^{-1} for the asymmetric stretch and at 1404 and 1375 cm^{-1} for the symmetric stretch. The separations (Δ) between ν_{asym} (CO_2) and ν_{sym}(CO_2) are 152 and 181 cm^{-1}, respectively. Complex **2** shows the characteristic bands of the carboxylate group at 1555 cm^{-1} for the asymmetric stretch and at 1417 and 1378 cm^{-1} for the symmetric stretch. The Δ values are 138 and 177 cm^{-1}, respectively. The respective Δ values in **1** and **2** reflect the fact that the carboxylate groups of HO−BDC function in two different coordination fashions, which are consistent with the crystal structures.

Structural Description of 1. Single-crystal X-ray diffraction analysis reveals that **1** is a three-dimensional network consisting of well-isolated one-dimensional metal/oxygen chains bridged by hydroxyl groups and HO−BDC along with gauche bime. The asymmetric unit contains two crystallographically independent Co^{II} ions (Figure 1). Co1 is in a distorted octahedral geometry, with four carboxylate oxygen atoms from different HO−BDC units occupying the equatorial basal plane and two μ_3-OH at the apical sites [O1−Co1−O1B = 162.7(2)°], whereas Co2 adopts a distorted trigonal-bipyramidal geometry surrounded by four oxygen and one nitrogen atoms. Two carboxylate oxygen atoms (O2, O3B) and one hydroxyl oxygen atom (O1A) comprise the equatorial plane, and the other hydroxyl oxygen atom (O1) and the nitrogen atom (N1) from gauche bime occupy the axial positions [O1−Co2−N1 = 175.38(16)°]. Co1 and Co2 are displaced by about 0.1021 and 0.0792 Å, respectively, from the equatorial planes toward the axial donor atoms. The

(16) (a) Liao, Y. C.; Liao, F. L.; Chang, W. K.; Wang, S. L. *J. Am. Chem. Soc.* **2004**, *126*, 1320. (b) Wang, Y.; Yu, J. H.; Guo, M.; Xu, R. R. *Angew. Chem., Int. Ed.* **2003**, *42*, 4089. (c) Neeraj, S.; Natarajan, S.; Rao, C. N. R. *Chem. Commun.* **1999**, 165. (d) Ayyappan, P.; Evans, O. R.; Lin, W. B. *Inorg. Chem.* **2002**, *41*, 3328.

(17) (a) Wang, X. L.; Qin, C.; Wang, E. B.; Xu, L.; Su, Z. M.; Hu, C. W. *Angew. Chem., Int. Ed.* **2004**, *43*, 5036. (b) Liu, Y. H.; Lu, Y. L.; Wu, H. C.; Wang, J. C.; Lu, K. L. *Inorg. Chem.* **2002**, *41*, 2592. (c) Shi, Z.; Li, G. H.; Wang, L.; Gao, L.; Chen, X. B.; Hua, J.; Feng, S. H. *Cryst. Growth Des.* **2004**, *4*, 25.

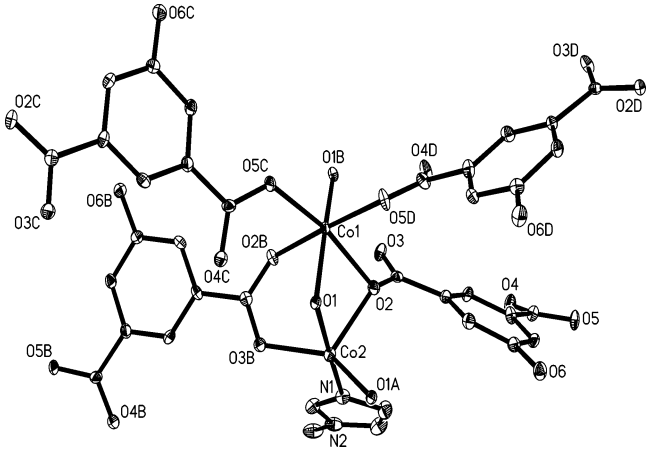

Figure 1. Perspective view of the asymmetric unit of **1** with 30% probability ellipsoids. Only one-half of the gauche bime ligand is shown for clarity.

Co−O and Co−N bond distances are all within the normal ranges.[5a,18] The Co1−O1−Co2 and Co1−O2−Co2 bond angles are 97.5° and 90.9°, respectively. HO−BDC acts as a μ_4-bridge (Chart 2a), linking four Co^{II} centers through a monodentate carboxylate and a μ_2,η^3-carboxylate group. The hydroxyl group in HO−BDC neither takes part in coordination nor is involved in hydrogen-bonding interactions, which is very different from other metal−OH−BDC compounds.[9b] Thus, Co1 and a symmetrically related pair Co2 and Co2A are connected by two μ_3-OH groups and three oxygen atoms from two μ_2,η^3-carboxylate groups to form a trinuclear subunit with Co1−Co2, Co1−Co2A, and Co2−Co2A distances of 3.121, 3.710, and 3.076 Å, respectively. Each unit is connected reversely through sharing of a μ_3-OH and a gauche bime bridge to generate a one-dimensional chain along with μ_2,η^3-carboxylate groups (Figure 2). As previously demonstrated for the cobalt hydroxyl derivatives,[19] the arrangements about the Co2 centers sharing the μ_3-OH groups are related to ferromagnetic coupling, whereas antiferromagnetic exchanges occur between Co1 and Co2, as well as between Co1 and Co2B. As for Co1 and Co2A, they are connected through sharing of only one vertex of a distorted octahedron (Co1) and a distorted trigonal-bipyramid (Co2) with a large Co1−O1−Co2A angle (132.63°); the corresponding exchange angle also implies antiferromagnetic coupling.[19a] On the other hand, the Co1−Co2A separation of 3.710 Å is quite longer than the Co2−Co2A and Co1−Co2 distances (3.076 and 3.121 Å), and according to the empirical Bloch law $J = d^{-10}$,[19d] the AF coupling between Co1−Co2A is about 1 order of magnitude less than the AF coupling between Co1−Co2 and can be neglected for simplification. Therefore, the chain can be approximately simplified as a zigzag cobalt chain along −Co2A−Co2−Co1−Co2B− with F/AF/AF magnetic interactions (as described in the Magnetic Properties section). The dihedral angle between the two imidazolyl rings in gauche bime is 28.7°; the Co2−Co2B distance separated by bime is 4.099 Å. Thus, the gauche conformation of bime plays an important role in the formation of the chain. The adjoining chains are further extended into a three-dimensional channel-like framework through the monodentate carboxylate group of HO−BDC coordinating to Co1 along different directions, where the shortest Co−Co interchain distance is 9.993 Å (Figure 3). It should be emphasized that the gauche bime lies in the channel and has significant effect on extending the interchain distances.

Structural Description of 2. 2 is also a three-dimensional framework based on one-dimensional chains from metal centers bridged by hydroxyl groups, HO−BDC, and gauche bime, but the bridging fashions of HO−BDC and the coordination environments of the metal centers are different from those in **1**. HO−BDC behaves in a μ_3-bridging mode linking three Cu^{II} ions by a monodentate carboxylate and a μ_2,η^2-carboxylate group (Chart 2b). The coordination environments of two crystallographically independent metal ions

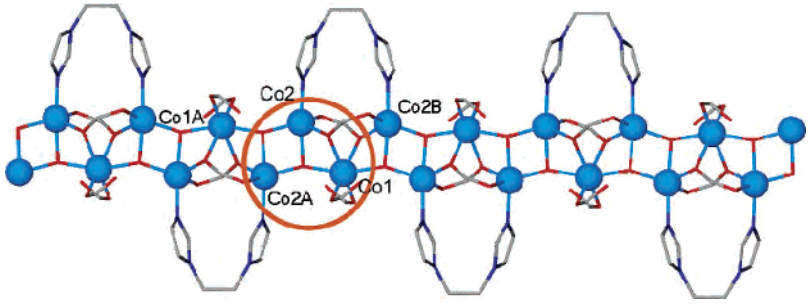

Figure 2. View of the 1D chain of **1**, with the trinuclear subunit exhibited in the orange loop.

Chart 2. HO−BDC Coordination Modes in (a) **1** and (b) **2**

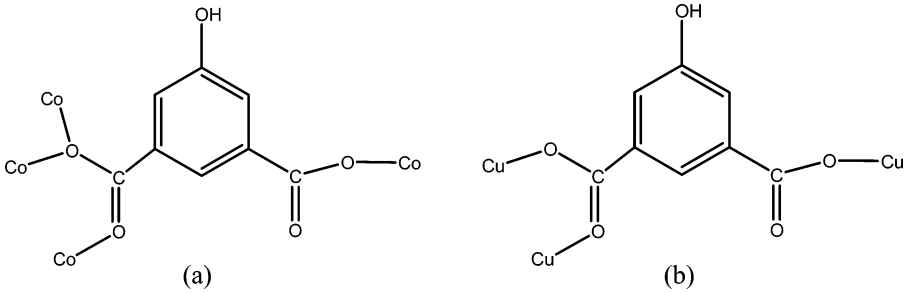

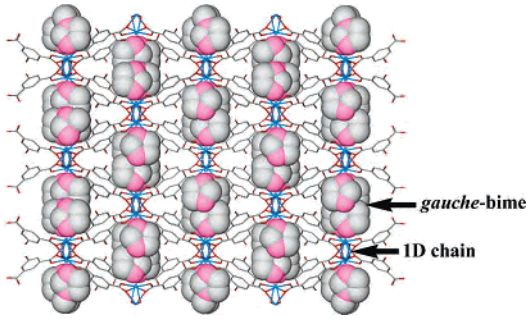

Figure 3. View of a 3D framework derived from 1D chains linked by HO−BDC with gauche bime ligands occupying void space along the *c* axis in **1**.

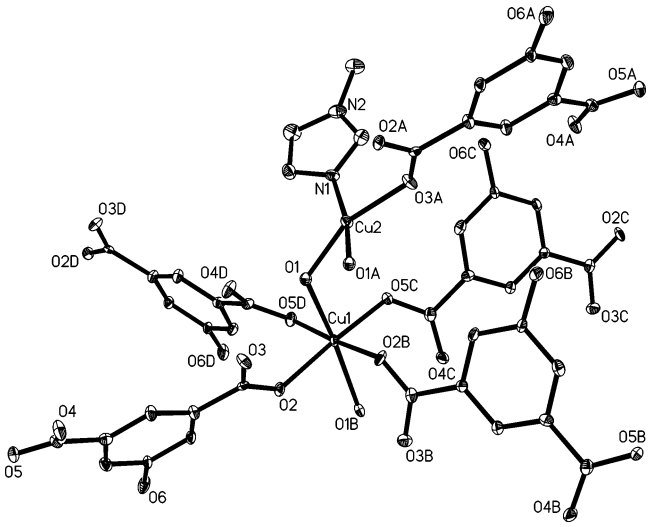

Figure 4. Perspective view of the asymmetric unit in **2**. The thermal ellipsoids are at the 30% probability level, and only one-half of the gauche bime ligand is shown for clarity.

(Cu1 and Cu2) are shown in Figure 4. Cu1 adopts a Jahn−Teller elongated octahedral coordination geometry in which two μ_3-OH oxygen atoms stand at the apical positions [Cu1−O1 = 2.336(5) Å, O1−Cu1−O1B = 167.6(3)°] and four carboxylate oxygen atoms comprise the equatorial plane [Cu1−O2 = 2.024(4) Å, Cu1−O5C = 1.973(4) Å]. However, Cu2 is in a square-planar geometry by coordinating to two μ_3-OH oxygen atoms, one carboxylate oxygen atom, and one nitrogen atom from the gauche bime ligand. The cis angles are in the range from 80.6(2) ° to 99.1(2)°. Cu1 and Cu2 are approximately coplanar with the planes defined by equatorial atoms with deviations of 0.0675 and 0.2173 Å, respectively. Similarly to those in **1**, μ_3-OH and η^2-carboxylate groups of the HO−BDC bridge three Cu^{II} ions (Cu1, Cu2, and Cu2A) to form a basic building unit of **2**. Such units are extended into a one-dimensional chain by μ_3-OH and gauche bime with Cu1−Cu2, Cu1−Cu2A, Cu2−Cu2A, and Cu2A−Cu2H distances of 3.766, 3.184, 2.925, and 4.679 Å, respectively (Figure 5). If the Cu1−Cu2 and Cu2A−Cu2H interactions are neglected, the one-dimensional configuration can be simplified into a zigzag metal chain. If these interactions are not neglected, it can be viewed as an alternating 1D chain as in **1**. The dihedral angle between the two imidazolyl rings of gauche bime is 36.3°, which is larger than that in **1**. HO−BDC further extends the one-dimensional chain into a three-dimensional network through the monodentate carboxylate group of HO−BDC coordinating to Cu1 along different directions (Figure 6). The nearest metal−metal distance between adjacent chains is 9.706 Å, which is shorter than that in 1.

Magnetic Properties. (i) Complex 1. Magnetic measurements were performed on a sample containing a collection of very small block single crystals with random orientations. Hysteresis loops of **1** at 1.77 and 1.9 K were measured using a Parafilm-constrained sample and an eicosane-constrained sample, respectively. The molar magnetic susceptibility of compound **1** per Co_3 unit in the temperature range 130−300 K obeys the Curie−Weiss law [$\chi_m = C/(T - \theta)$], giving $C = 9.03(6)$ cm^3 mol^{-1} K and $\theta = -83(1)$ K (Figure 7). The C value corresponds to $g = 2.53$. The large negative value of θ suggests a dominant antiferromagnetic coupling between Co ions within the chain, although the single-ion behavior of octahedral Co(II) could also have partially contributed to the negative θ, but not to such a large value. As the temperature is decreased, the $\chi_m T$ value decreases gradually and reaches a minimum at about 69 K (5.00 cm^3 mol^{-1} K); it then increases abruptly below 30 K, suggesting a ferrimagnetic-like character. Because of the lack of an appropriate analytical expression for an anisotropic model of this complicated system, a Heisenberg model could be used approximately based on the structure data: Co1 is in a distorted octahedral geometry, and Co2 adopts a distorted trigonal-bipyramidal geometry; therefore, the anisotropy of the Co(II) ion can be attributed to an assumed isotropic g parameter. Furthermore, the complicated chain was approximated as a zigzag linear cobalt chain along −Co2A−Co2−Co1−Co2B− with alternating F/AF/AF interactions to estimate the magnetic exchange between adjacent Co^{II} ions, if the moments of all Co2 ions are spin up and those of Co1 are spin down, based on the connection of Co ions and ref 19. The magnetic susceptibility data above 40 K can be fitted well by an alternating 1D-chain ($S = {}^3/_2$) model ($H = -J_1\sum(S_{3i}S_{3i+1} + S_{3i+1}S_{3i+2}) - J_2\sum S_{3i-1}S_{3i}$, where J_1 is the intrachain coupling between Co1 and Co2 and J_2 is the intrachain coupling between Co2 ions),[20] giving $J_1 = -35.7(5)$ cm^{-1} $= -51.4$ K, $J_2 = +13.9(3)$ cm^{-1} $= 20$ K, $g = 2.528(8)$, and $R = 1.3 \times 10^{-4}$ $\{R = \sum[(\chi_m T)_{obsd} - (\chi_m T)_{calcd}]^2/\sum[(\chi_m T)_{obsd}]^2\}$. The ferrimagnetic-like behavior can be suggested to arise from the competitive ferromagnetic coupling between Co2 ions and the AF coupling between Co1 and Co2 ions, resulting in a net moment of one Co2 ion per Co_3 unit.

The field dependence of the magnetization of **1** at 1.77 and 1.90 K is shown in Figure 8. The magnetization at 70 kOe is 2.35 Nβ per Co_3 unit, consistent with the moment of

(18) Manson, J. L.; Arif, A. M.; Miller, J. S. *Chem. Commun.* **1999**, 1479.
(19) (a) Livage, C.; Egger, C.; Férey, G. *Chem. Mater.* **1999**, *11*, 1546. (b) Huang, Z. L.; Drillon, M.; Masciocchi, N.; Sironi, A.; Zhao, J. T.; Rabu, P.; Panissod, P. *Chem. Mater.* **2000**, *12*, 2805. (c) Kumagai, H.; Kepert, C. J.; Kurmoo, M. *Inorg. Chem.* **2002**, *41*, 3410. (d) Angelov, S.; Drillon, M.; Zhecheva, E.; Stoyanova, R.; Belaiche, M.; Derory, A.; Herr, A. *Inorg. Chem.* **1992**, *31*, 1514.
(20) Abu-Youssef, M. A. M.; Drillon, M.; Escuer, A.; Goher, M. A. S.; Mautner, F. A.; Vicente, R. *Inorg. Chem.* **2000**, *39*, 5022.

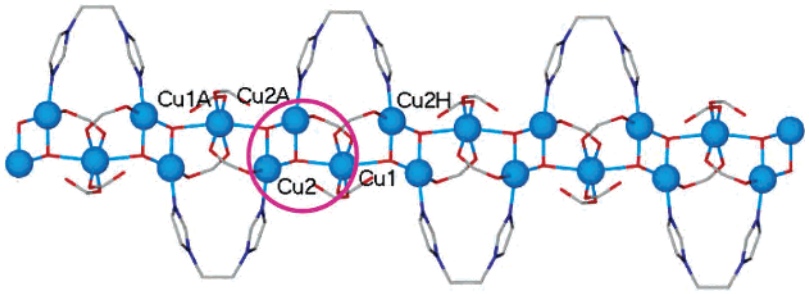

Figure 5. View of the 1D chain in **2**, with the trinuclear unit exhibited in the purple loop.

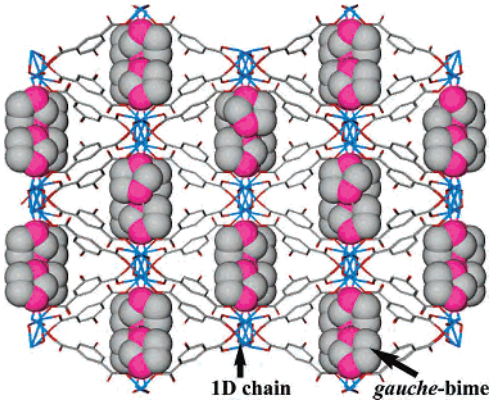

Figure 6. View of a 3D framework derived from 1D chains linked by HO−BDC along the *c* axis in **2**.

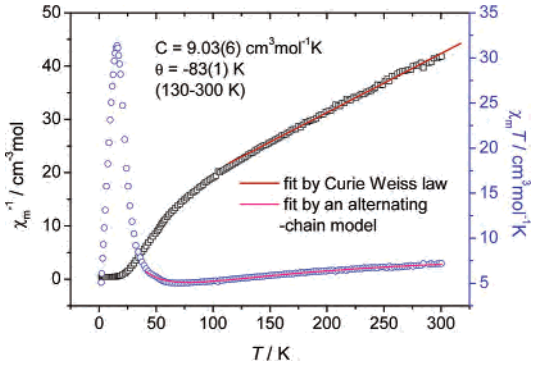

Figure 7. Temperature dependence of the magnetic susceptibility χ_m^{-1} and $\chi_m T$ of **1**.

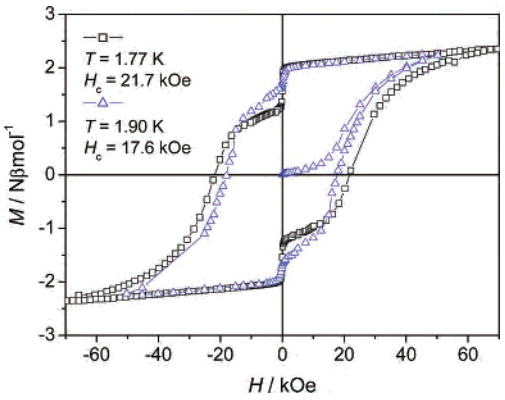

Figure 8. Field dependence of the magnetization of 1 measured at 1.77 and 1.90 K, using MagLab2000 and SQUID instruments with the sample constrained in Parafilm and eicosane, respectively.

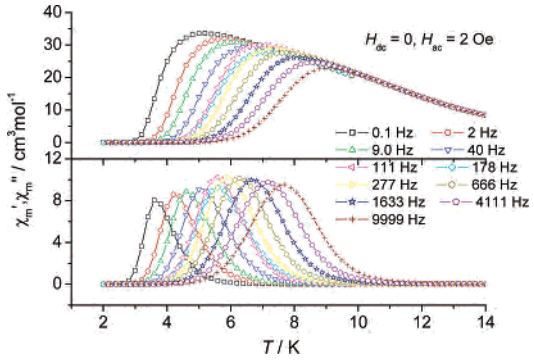

Figure 9. Temperature dependence of the real (top) and imaginary (bottom) components of the ac susceptibility in zero dc field with an ac field 2 Oe in the frequency range of 0.1−9999 Hz. The lines are guides for the eye.

one Co(II) ion. This also suggests that the noncompensating resultant moment is from both F and AF exchange interactions. A considerably large hysteresis loop is observed below 2.0 K, giving a coercive field of 21.7 kOe at 1.77 K and 17.6 kOe at 1.90 K, respectively. The above dc magnetic data for **1** seem to support a ferrimagnetic-like 3D hard magnetism. The magnetic behavior is reminiscent of that observed in some homometallic molecular ferrimagnets[5b,8] and the high coercivity in some Co(II) and Mn(III) compounds.[21] Figure 8 also shows a sharp drop of magnetization at zero and weak field. Although the temperatures are not exactly the same, this step seems to have different amplitudes for the two measurements. The larger jump at 1.77 K can be mainly attributed to rotation of the powder sample simply constrained in Parafilm.

Field-cooled and zero-field-cooled magnetic susceptibility at fields of 10 and 50 Oe (Figure S1) show the irreversibility below ca. 4.5−4.0 K, suggesting possible spin-glass or superparamagnetic behavior.

The ac magnetic susceptibility data for 1 collected in the frequency range of 0.1−9999 Hz using MagLab2000 and MPMS-XL5 SQUID instruments show a strong frequency dependence in both the real (χ') and imaginary (χ'') parts (Figure 9). The shift of peak temperature (T_P) of χ' can be quantified as $\phi = (\Delta T_P/T_P)/\Delta(\log f) = 0.15$, which is much larger than that for a typical spin glass (where ϕ is around 0.01), but more typical for superparamagnetic blocking.[22] Moreover, although the frequency dependence can be fitted by the conventional critical scaling law of the spin dynamics

(21) (a) Kurmoo, M. *Chem. Mater.* **1999**, *11*, 3370. (b) Rittenberg, D. K.; Sugiura, K.; Sakata, Y.; Mikami, S.; Epstein A. J.; Miller, J. S. *Adv. Mater.* **2000**, *12*, 126.

(22) Mydosh, J. A. *Spin Glasses: An Experimental Introduction*; Taylor & Francis: London, 1993.

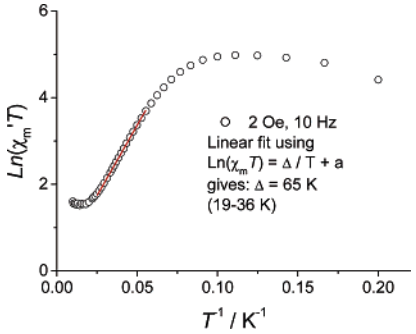

Figure 10. Semilogarithmic plot of χ'_mT vs $1/T$. The data were obtained from ac measurements at 2 Oe and 10 Hz at zero dc field.

as described by $\tau = \tau_0[(T_P - T_f)/T_f]^{-z\nu}$, where $\tau = 1/(2\pi f)$, giving $\tau_0 = 8 \times 10^{-2}$ s, $z\nu = 3.7$, and $T_f = 2.1$ K (Figure S2a; T_f is the freezing temperature for a spin-glass phase), the obtained $z\nu$ value of 3.7 is outside the range (from 4 to 12) for various spin glasses. Meanwhile, the frequency dependence of T_P can be fitted well to an Arrhenius law of the form $\tau = \tau_0 \exp(\Delta E/k_BT)$, with physically reasonable values of $\tau_0 = 1.1 \times 10^{-9}$ s and $\Delta E/k_B = 76(1)$ K (Figures 9 and S2b). At 5.9 K, around the cusp of the out-of-phase signal χ'', a close semicircle Cole−Cole diagram was obtained (χ'' vs χ' in Figure S3), which can be fitted by a generalized Debye model with an α parameter of 0.50, indicating a large distribution in relaxation time. In short, the frequency dependence of the linear ac susceptibility suggests a superparamagnetic-like behavior. The magnetic relaxation behavior is quite similar to that observed in single-molecule magnets, as well as in molecular magnetic nanowires, where the energy barrier originates from the magnetic anisotropy.[1,2]

The zero field ac magnetic susceptibility data are also shown in $\ln(\chi'_mT)$ vs $1/T$ form in Figure 10. The linear behavior observed in the $\ln(\chi'_mT)$ vs $1/T$ plot over the range 19−36 K indicates a strong Ising-like anisotropy. The high-temperature deviation should be attributed to the population of higher-energy electronic levels of the Co(II) ions; and the low-temperature deviation below 18 K from the linear regime is consistent with a geometrical limitation of the correlation length due to the presence of defects; this type of phenomenon was observed and analyzed in refs 23 and 24. The fitting of the data in the linear regime gave a slope of 65 K (with $R = 0.9998$), which corresponds to a barrier.[23−24] The gap in the relaxation time is 76 K (Figures 9 and S2b), which is less than twice the barrier (65 K) in the $\ln(\chi'_mT)$ vs $1/T$ plot. Therefore, this compound is in the finite-size limit, where the correlation length of the system is larger than the chain length. This is valid independently of the microscopic model. The energy necessary to reverse the magnetization of an individual magnetic unit composing the chain is thus obtained as $76 - 65 = 11$ K. This value quantifies the anisotropy.

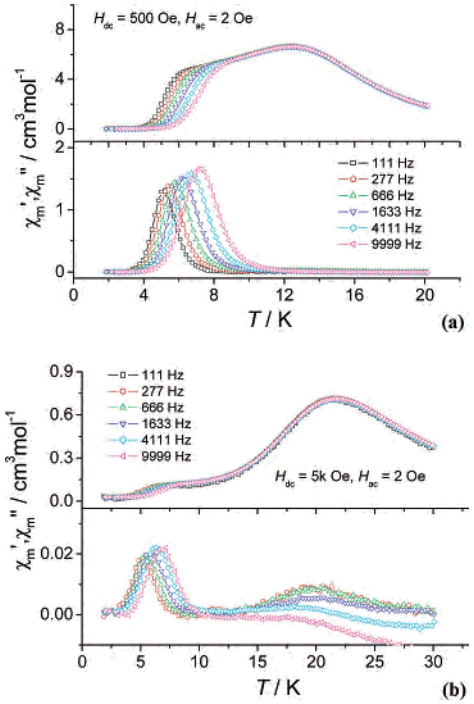

Figure 11. Temperature dependence of the real and imaginary components of the ac susceptibility of 1 at H_{dc} = (a) 0.5 and (b) 5 kOe with an ac field of 2 Oe in the frequency range of 111−9999 Hz. The lines are guides for the eye.

Given that 11 K ≪ 63 K, this is demonstrates that this compound is not in the Ising limit as in refs 2a and 24.

Another key thermodynamic feature to be associated with finite-size effects was predicted and experimentally observed in CoPhOMe:[24] A static dc field separates the total ac susceptibility into contributions from the bulk infinitely long chains, the finite chains of segment length L, and the spins at the end of the chains. Experimentally, a high-temperature frequency-independent peak and a low-temperature frequency-dependent peak were observed. Figure 11 shows the temperature dependence of the real and imaginary components of the ac susceptibility for 1 in 0.5 and 5 kOe applied static fields with an ac field of 2 Oe in the frequency range of 111−9999 Hz. The in-phase component (χ'_m) under the 0.5 kOe dc field clearly displays a frequency-independent peak at 12.5 K and another frequency-dependent peak above 5 K. The higher dc field of 5 kOe moves the high-temperature frequency-independent peak to 22 K. This experimental observation of a double-peaked feature in susceptibility in the external applied field for **1** (Figure 11) is quite similar to the theoretical prediction and observed behavior shown in CoPhOMe,[24b] giving further evidence for finite-size effects.

According to the above data and discussion, finite-size effects are surely present in the nominally pure compound.

On the other hand, the second-harmonic nonlinear ac susceptibility was observed in the frequency range of 277−4111 Hz at zero dc field as shown in Figure 12a, although it is 3 orders of magnitude smaller than the linear χ_{ac} and disappears at high frequency. The second nonlinear ac susceptibilities measured at 0.5 kOe are negligibly small, essentially at noise level (Figure 12b). The presence of the

(23) Coulon, C.; Clérac, R.; Lecren, L.; Wernsdorfer, W.; Miyasaka, H. *Phys. Rev. B* **2004**, *69*, 132408.
(24) (a) Bogani, L.; Caneschi, A.; Fedi, M.; Gatteschi, D.; Massi, M.; Novak, M. A.; Pini, M. G.; Rettori, A.; Sessoli, R.; Vindigni, A. *Phys. Rev. Lett.* **2004**, *92*, 207204. (b) Bogani, L.; Sessoli, R.; Pini, M. G.; Rettori, A.; Novak, M. A.; Rosa, P.; Massi, M.; Fedi, M. E.; Giuntini, L.; Caneschi, A.; Gatteschi, D. *Phys. Rev. B* **2005**, *72*, 064406.

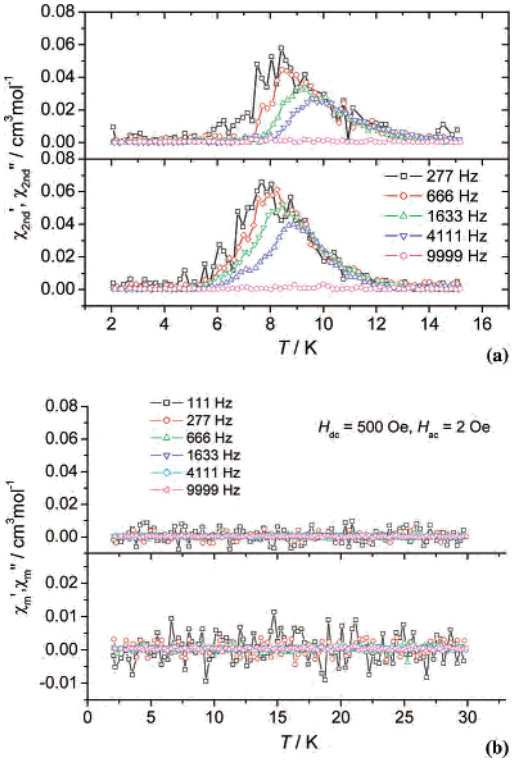

Figure 12. Temperature dependence of the real and imaginary components of the second-harmonic ac susceptibility for **1** in (a) zero applied static field and (b) 0.5 kOe field with an ac field of 2 Oe in the frequency range of 111−9999 Hz.

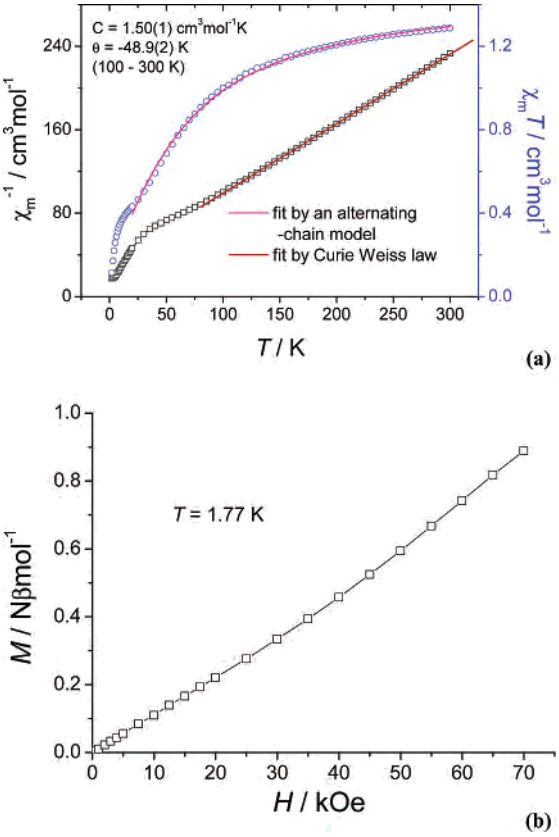

Figure 13. (a) Temperature dependence of the magnetic susceptibility χ_m^{-1} and $\chi_m T$ of **2**. (b) Field dependence of magnetization of **2** at 1.77 K.

very weak even harmonic response of χ' and χ'' at zero dc field might suggest a small spontaneous magnetization[25] in **1**, possibly due to the quite weak interchain interaction (separation of 1 nm) and/or impurities of a very small part of the ferromagnetic component. The peak of the second harmonic of the ac susceptibility in **1** is fully suppressed with the application of a 0.5 kOe field, in contrast to the enhancement of the signal in a small dc field for $[MnTPP]^+$-$[TCNE]^-$ solvents.[26]

(ii) Complex 2. For comparison, complex **2**, a structural analogue of **1**, was studied, and the temperature dependence of χ_m per Cu_3 unit shown in Figure 13a. The magnetic susceptibility data of 2 in the temperature range 100−300 K obeys the Curie−Weiss law, giving $C = 1.50(1)$ cm^3 mol^{-1} K and $\theta = -48.9(2)$ K. The C value corresponds to $g = 2.30$. First, the chain was simplified as a uniform linear $S = {}^1/_2$ chain to obtain insight into the intrachain coupling between Cu(II) ions; the magnetic susceptibility data above 50 K can be fitted well by a Fisher 1D chain model ($H = -JS_iS_j$, intrachain coupling J),[27] giving $J = -55.0(2)$ cm^{-1} $= -79.1$ K, $g = 2.287(1)$, and $R = 5.8 \times 10^{-6}$. Fitting the same set of data using the model given by Weng and modified by Hiller with the same Hamiltonian gives the best-fit parameters:[28] $J = -44.4(1)$ cm^{-1} $= 63.9$ K and $g = 2.305(1)$ with $R = 4.7 \times 10^{-6}$. Apparently, an overall antiferromagnetic coupling is dominant within the Cu chain. If an alternating 1D chain ($S = {}^1/_2$) model[20] was used considering the similar metal connectivities in **1** and **2** [$H = -J_1\sum(S_{3i}S_{3i+1} + S_{3i+1}S_{3i+2}) - J_2\sum S_{3i-1}S_{3i}$, where J_1 is the intrachain coupling between Cu1 and Cu2 and J_2 is the intrachain coupling between Cu2 ions], the magnetic susceptibility data of **2** above 20 K can be fitted well, giving $J_1 = -78(1)$ cm^{-1}, $J_2 = -16(1)$ cm^{-1}, $g = 2.299(4)$, and $R = 7.9 \times 10^{-5}$. In any event, the interactions of neighboring Cu1−Cu2 and Cu2−Cu2 atoms are all antiferromagnetic in character. The field-dependent magnetization of **2** at 1.77 K (Figure 13b) shows a slow nearly linear increase with increasing field, and the magnetization at 70 kOe is just 0.89 Nβ per Cu_3 unit, far from saturation, supporting the antiferromagnetic behavior.

Conclusions

In summary, two novel three-dimensional frameworks consisting of well-isolated metal/oxygen chains are obtained from the hydrothermal reactions of 1,2-bis(imidazol-1′-yl)-ethane and 5-hydroxyisophthalic acid with $Co(NO_3)_2{\cdot}6H_2O$ and $Cu(NO_3)_2{\cdot}3H_2O$. Complex **1** shows slow magnetic relaxation and a large hysteresis at low temperature and

(25) Gîrtu, M. A.; Wynn, C. M.; Fujita, W.; Awaga, K.; Epstein, A. J. *Phys. Rev. B* **1998**, *57*, R11058 and references therein.
(26) Etzkorn, S. J.; Hibbs, W.; Miller, J. S.; Epstein, A. J. *Phys. Rev. Lett.* **2002**, *89*, 207201.
(27) Fisher, M. E. *Am. J. Phys.* **1964**, *32*, 343.
(28) (a) Weng, C. Y. Ph.D. Thesis, Carnegie Institute of Technology, Pittsburgh, PA, 1968. (b) Hiller, W.; Strahle, J.; Datz, A.; Hanack, M.; Hatfield, W. E.; ter Haar, L. W.; Guetlich, P. *J. Am. Chem. Soc.* **1984**, *106*, 329.

displays distinct finite-size effects. Complex **2** displays antiferromagnetic chain behavior.

Acknowledgment. The authors acknowledge financial support from the National Science Fund for Distinguished Young Scholars (20325106, 20125104), NSFC 90206040, 20221101, and 20490210; NSF of Fujian Province (E0520003); and "One Hundred Talent Project" from CAS. G.S. thanks Dr. R. Clérac (Centre de Recherche Paul Pascal, CRPP-CNRS, France) for valuable discussions.

Supporting Information Available: Some magnetic plots and crystallographic information files (CIF) of two compounds are available free of charge via the Internet at http://pubs.acs.org.

IC050999X